Electron magnetic resonance in interacting ferromagnetic-metal nanoparticle systems: experiment and numerical simulation

2010 J. Phys.: Condens. Matter 22 016005

(http://iopscience.iop.org/0953-8984/22/1/016005)

J. Phys.: Condens. Matter **22** (2010) 016005 (10pp) doi:10.1088/0953-8984/22/1/016005

Electron magnetic resonance in interacting ferromagnetic-metal nanoparticle systems: experiment and numerical simulation

Chiharu Mitsumata[1], Satoshi Tomita[2], Masayuki Hagiwara[3] and Kensuke Akamatsu[4]

[1] Production System Laboratory, Hitachi Metals Ltd, 6010 Mikajiri, Kumagaya, Saitama 360-0843, Japan
[2] Graduate School of Materials Science, Nara Institute of Science and Technology (NAIST), 8916-5 Takayama, Ikoma, Nara 630-0192, Japan
[3] KYOKUGEN (Center for Quantum Science and Technology under Extreme Conditions), Osaka University, 1-3 Machikaneyama, Toyonaka, Osaka 560-8531, Japan
[4] FIRST, Konan University, and PRESTO, Japan Science and Technology Agency, 7-1-20 Minatojima-minami, Chuo, Kobe 650-0047, Japan

E-mail: chiharu_mitsumata@hitachi-metals.co.jp and tomita@ms.naist.jp

Received 28 September 2009, in final form 6 November 2009
Published 2 December 2009
Online at stacks.iop.org/JPhysCM/22/016005

Abstract
We have studied electron magnetic resonance (EMR) in ferromagnetic-metal nanoparticle systems which show promise as a component of left-handed metamaterials. Metallic Ni nanoparticles of about 8 nm in diameter are embedded in polymer films. When the average distance between the nanoparticles is decreased, we observed that the EMR signal shifts and broadens. Theoretical analyses based on micromagnetics simulation confirm that the shift of the signal is traced back to an increase in the magnetic dipole field in the nanoparticle systems due to the decrease in interparticle distance. Moreover, the simulation reveals that the perpendicular component of the dipolar field causes the broadening of the signal. The present study demonstrates that a dynamic analysis of the magnetization, with an explicit treatment of the magnetic dipole interactions, is necessary for a thorough understanding of the EMR and magnetic permeability of interacting nanoparticle systems.

1. Introduction

Metamaterials consisting of artificial building blocks much smaller than the wavelengths of electromagnetic (EM) waves are a rich and rapidly growing area in microwave optics and photonics [1]. Left-handed metamaterials (LHMs), which mimic negative electric permittivity (ϵ) and magnetic permeability (μ) simultaneously, are of particular interest because they show intriguing EM responses, e.g. negative refraction and inverse Doppler shift [2]. The negative refraction has led to the consideration of LHMs, or negative index of refraction metamaterials, for applications in perfect lenses [3] and compact optical components [4]. Moreover, metamaterials having positive but finite values of μ between 0 and 1 open the door to an EM cloak [5].

A tailored value of μ, even of negative μ, is obtained using magnetic resonance. Structural magnetic resonance with split-ring resonators, which are made of a non-magnetic metal such as Cu, is a well-known technique to achieve negative μ in microwave regions [6, 7]. On the other hand, an alternative route using intrinsic magnetic resonance of ferromagnetic metals, for example, Fe, Co and Ni, has been plotted [8]. Using electron magnetic resonance (EMR) in the metals, negative μ is obtained around an EMR frequency [9]. The resonance frequency tunability with an external magnetic field is expected to be a significant advantage of this route. It is, however, necessary to miniaturize the ferromagnetic-metals, i.e. prepare ferromagnetic-metal nanoparticle systems, in order to suppress the eddy-current losses.

In spite of intensive studies [10–12], the EMR in ferromagnetic-metal nanoparticle systems is poorly understood. The magnetic behavior and dynamics of magnetization in nanoparticle systems are dependent both on single-particle properties, such as magnetocrystalline or shape anisotropies of

a particle [13–17], and on interparticle interactions [18, 19]. For magnetically isolated particles with negligible interaction, one needs to consider only single-particle properties. In contrast, in the case of strongly interacting particle systems, an explicit treatment of the interactions is necessary [20, 21].

Magnetic interactions between nanoparticles strongly affect the position and linewidth of the EMR spectra [22–25]. In nanoparticle systems, we usually consider two kinds of interactions: long range magnetic dipole interactions and short range direct/indirect exchange interactions [26–28]. The relative importance of each to EMR depends on the particle diameter (d) and center-to-center interparticle separation (r) [29]. Therefore, from an experimental point of view, nanoparticles with independently controlled d and r are necessary to study EMR in an interacting nanoparticle system [30].

Recently, we succeeded in embedding metallic Ni nanoparticles into polymer thin films in a controlled manner [31–34]. A significant feature of this technique is a decrease in r of the nanoparticles, which maintain a fixed d at the level of several nanometers. This is not achieved through particle manipulation, but by shrinking the polymer matrices, which results in a good model system for experimental studies of the magnetic interaction in single-domain ferromagnetic-metal nanoparticle systems. We have reported that the EMR signals of the Ni nanocomposite film strongly depend on d and r of Ni nanoparticles [32]. Nonetheless, the exact mechanics of the interactions affecting the resonance condition are still unclear. A detailed theoretical consideration is thus indispensable.

From a theoretical point of view, the resonance absorption of microwave power by a film consisting of a lattice of point magnetic dipoles has been studied so far [35, 36]. The resonance condition of the thin films is well known to be described by Kittel's equations [37]. Kittel's equations are enough to explain the EMR field of nanoparticle systems embedded in thin films. The equations are, however, inadequate for discussing the linewidth of the signal [32]. The evaluation of the EMR linewidth is critical in an estimation of μ of nanoparticle systems. It is thus essential to directly solve the Landau–Lifshitz–Gilbert (LLG) motion equation of the magnetization. Many numerical models have been proposed. A direct solution of the LLG equation was discussed for larger magnetic particles, in which several magnetic domains exist [24, 38]. Although the set of single-domain particles with random direction of magnetization was investigated [39], the model does not include the dipole interactions between the particles. These models are thus insufficient in a study of single-domain nanoparticle systems with mutual dipolar interaction. Very recently, we constructed a numerical model for the nanoparticle systems and evaluated μ of the system [40]. The comparison with experimental EMR results is, however, lacking.

The purpose of this work is to increase knowledge about the dynamics of the magnetization of particles in interacting single-domain ferromagnetic-metal nanoparticle systems and to understand the EMR of the systems. A computer simulation, in which the dipolar interactions between the particles are considered explicitly, has been conducted in order to interpret the experimental EMR results. In particular, we focus our attention on the resonance field and its linewidth. This paper is organized as follows; the following two sections describe the theoretical background (section 2) and simulation framework (section 3) for EMR in nanoparticle systems. We briefly describe experimental procedures in section 4. Section 5 shows experimental and numerical results followed by a discussion. Finally, we conclude by highlighting the advantages of our numerical model.

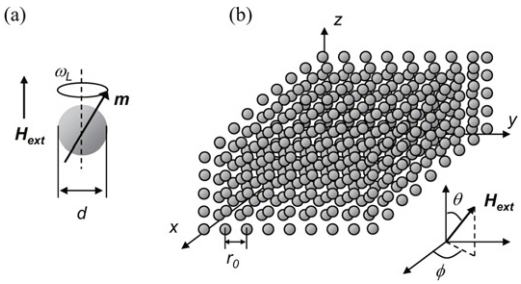

Figure 1. Schematic illustrations of (a) a magnetically isolated spherical nanoparticle and (b) a 3D array of interacting nanoparticles.

2. Theoretical background

Let us start with the EMR in a magnetically isolated spherical Ni nanoparticle. We consider a nanoparticle with a total magnetic moment $\boldsymbol{m}$ as illustrated in figure 1(a). Under an external magnetic field H_{ext}, the moment $\boldsymbol{m}$ precesses at an angular frequency ω_{L} (the Larmor frequency). The ω_{L} is expressed as $\omega_{\mathrm{L}} = |\gamma| H_{\mathrm{int}}$ [37], where H_{int} is an internal magnetic field that is equal to H_{ext} for an ideal spherical particle and γ is the gyromagnetic ratio that is related to the g value by $\gamma = -2\pi g \mu_{\mathrm{B}}/h$. Here, μ_{B} is the Bohr magneton and h is the Planck constant. On resonance, the particle magnetic moment precessing at ω_{L} absorbs a microwave with the same frequency ν ($2\pi\nu = \omega_{\mathrm{L}}$). EMR measurements are usually carried out by sweeping H_{ext} at a constant ν. The resonance condition is thus expressed simply as $H_{\mathrm{ext}} = H_{\mathrm{int}} = \omega_{\mathrm{L}}/|\gamma| = 2\pi\nu/|\gamma| = H_0$, where H_0 denotes the resonance field for the magnetically isolated spherical nanoparticle. For an isolated Ni nanoparticle measured at the X band (ν = 9–10 GHz), the resonance field H_0 is expected to be about 3000 Oe from ferromagnetic resonance in a bulk Ni sphere ($g = 2.21$) [37].

If the particle is non-spherical in shape, the resonance condition will be changed, i.e. $H_{\mathrm{ext}} \neq H_{\mathrm{int}}$, owing to the demagnetization field in the particle. However, we consider spherical Ni particles in this paper. The demagnetization field in the Ni particle is thus disregarded. The direction of magnetic moment $\boldsymbol{m}$ is treated as uniform in the particle. Additionally, Ni particles are small enough to be regarded as single-domain particles in this paper. These allow us the single-spin approximation for the total magnetic moment in the Ni nanoparticle in the following equations.

In an interacting particle system, we take the dipole interactions between the particles into consideration. The

dipolar field ($\boldsymbol{H}_{\rm dip}$) generated by a particle having $\boldsymbol{m}$ at distance $\boldsymbol{r}$ is described as

$$\boldsymbol{H}_{\rm dip} = -\frac{\boldsymbol{m}}{r^3} + \frac{3(\boldsymbol{m}\cdot\boldsymbol{r})\boldsymbol{r}}{r^5}. \tag{1}$$

Taking $\boldsymbol{H}_{\rm dip}$ into consideration, we may express the magnetic field applied to the interacting nanoparticle system by $\boldsymbol{H}_{\rm ext} + \boldsymbol{H}_{\rm dip}$. The resonance occurs when $\boldsymbol{H}_{\rm ext} = \boldsymbol{H}_0'$ which satisfies the resonance condition $|\boldsymbol{H}_{\rm ext} + \boldsymbol{H}_{\rm dip}| = |\boldsymbol{H}_0' + \boldsymbol{H}_{\rm dip}| = H_0$.

The form of equation (1) allows the calculation of the point dipole approximation. The validity of this approximation depends on the interparticle distance. If the interparticle distance is very small, equation (1) should be replaced by an equation including quadruple or higher-order interactions. Since the exact calculation of $\boldsymbol{H}_{\rm dip}$ is complicated, particularly for particles which are only slightly separated [41, 42], we accept the values with a simple discussion of the use of equation (1).

As expressed in equation (1), $\boldsymbol{H}_{\rm dip}$ gives long range interactions between particles. The exact formula of the dipolar field can be obtained by integrating equation (1). In the present investigation, we intend to analyze nanoparticle systems, in which the particle diameter is small enough and each magnetic particle can be regarded as a single domain. We thus use an approximation of the summation of the point dipole in the following. Using $\boldsymbol{m} = (m_x, m_y, m_z)$ and $\boldsymbol{r} = (r_x, r_y, r_z)$, the x, y, z components of the total dipolar field in the nanoparticle system $\boldsymbol{H}_{\rm dip}^{\rm total} = \sum \boldsymbol{H}_{\rm dip}$ are described, respectively, as

$$H_{\rm dip}^{{\rm total}(x)} = \sum\left[-\frac{m_x}{r^3} + \frac{3(m_x\cdot r_x + m_y\cdot r_y + m_z\cdot r_z)r_x}{r^5}\right], \tag{2}$$

$$H_{\rm dip}^{{\rm total}(y)} = \sum\left[-\frac{m_y}{r^3} + \frac{3(m_x\cdot r_x + m_y\cdot r_y + m_z\cdot r_z)r_y}{r^5}\right], \tag{3}$$

$$H_{\rm dip}^{{\rm total}(z)} = \sum\left[-\frac{m_z}{r^3} + \frac{3(m_x\cdot r_x + m_y\cdot r_y + m_z\cdot r_z)r_z}{r^5}\right]. \tag{4}$$

In the present experiments, nanoparticles are embedded in the surface layer of thin polymer films. For a rough approximation, it is acceptable to consider the thin composite layer as a two-dimensional (2D) infinite film. We assume that the magnetizations in particles are uniformly laid in the direction of an applied field. In other words, equations (2)–(4) can be calculated with the continuum approximation of magnetization. These calculations provide the simple aspects of dipole interaction in our composite film system.

Here, θ and ϕ are defined in figure 1(b); θ is the angle between the z axis and $\boldsymbol{H}_{\rm ext}$. When the external magnetic field $H_{\rm ext}$ is applied along the z axis, i.e. $\theta = 0°$, $\boldsymbol{m} = (0, 0, m_z)$ because we assume $H_{\rm ext} \gg H_{\rm dip}$ and $\boldsymbol{r} = (r_x, r_y, 0)$. Consequently, $H_{\rm dip}^x = H_{\rm dip}^y = 0$ and $H_{\rm dip}^z$ are expressed as

$$H_{\rm dip}^z = -\frac{m_z}{r^3} = -\frac{|\boldsymbol{m}|}{r^3}. \tag{5}$$

By integrating $H_{\rm dip}^z$ in equation (5) for the 2D array of the particles, the $H_{\rm dip}^{\rm total}$ can be calculated semi-quantitatively as

$$H_{\rm dip}^{\rm total} = \int_0^{2\pi}\int_{r_0}^{\infty} -\frac{|\boldsymbol{m}|}{r^3} r\,{\rm d}r\,{\rm d}\phi \propto -\frac{m}{r_0}, \qquad \theta = 0°. \tag{6}$$

On the other hand, when $H_{\rm ext}$ is applied along the x axis (the $\theta = 90°$ configuration), $\boldsymbol{m}$ is pointed in the x direction. $\boldsymbol{m} = (m_x, 0, 0)$ at $(r\cos\phi, r\sin\phi, 0)$ in a cylindrical coordinate generates the dipolar field $H_{\rm dip}^x$ which is represented by

$$H_{\rm dip}^x = -\frac{m_x}{r^3} + \frac{3(m_x r\cos\phi)(r\cos\phi)}{r^5} = \frac{(3\cos^2\phi - 1)m_x}{r^3}. \tag{7}$$

The dipolar field $H_{\rm dip}^z$ is equal to zero and $H_{\rm dip}^y$ becomes zero after integration. By integrating $H_{\rm dip}^x$ in equation (7) for the 2D array, we obtain $H_{\rm dip}^{\rm total}$ semi-quantitatively as

$$H_{\rm dip}^{\rm total} = \int_0^{2\pi}\int_{r_0}^{\infty} \frac{(3\cos^2\phi - 1)m_x}{r^3} r\,{\rm d}r\,{\rm d}\phi \tag{8}$$

$$\propto \frac{m}{2r_0}, \qquad (m_x = m) \qquad \theta = 90°. \tag{9}$$

As a result, the modified resonance condition $H_0' = H_0 - H_{\rm dip}^{\rm total}$ predicts that, owing to the dipolar field $H_{\rm dip}^{\rm total}$, H_0' at $\theta = 90°$ is smaller than H_0 and H_0' at $\theta = 0°$ is larger than H_0. Additionally, we notice that the absolute value of $H_{\rm dip}^{\rm total}$ at $\theta = 0°$ in equation (6) is twice as large as that at $\theta = 90°$ in equation (9). These equations are enough to quantitatively interpret the resonance field of the nanoparticle systems embedded in thin films [32]. However, information on the intensity and linewidth of the resonance is lacking. We thus need to carry out a dynamic analysis on the EMR of nanoparticle systems with the effect of the dipolar field.

3. Framework of model simulation

The numerical model is dynamically treated by solving the LLG motion equation of magnetization. The motion equation of magnetization in the ith Ni particle can be written as

$$\frac{{\rm d}\boldsymbol{m}_i}{{\rm d}t} = -\frac{\gamma}{1+\alpha^2}(\boldsymbol{m}_i \times \boldsymbol{H}_{\rm int}^i) - \frac{\alpha\gamma}{\boldsymbol{m}_{\rm s}(1+\alpha^2)}\{\boldsymbol{m}_i \times (\boldsymbol{m}_i \times \boldsymbol{H}_{\rm int}^i)\}, \tag{10}$$

where α is the Gilbert damping factor, which is phenomenologically introduced in the motion equation. The magnetic field $\boldsymbol{H}_{\rm int}^i$ includes the applied field $\boldsymbol{H}_{\rm ext}$ and the dipolar field $\boldsymbol{H}_{\rm dip}^{\rm total}$ as $\boldsymbol{H}_{\rm int} = \boldsymbol{H}_{\rm ext} + \boldsymbol{H}_{\rm dip}^{\rm total}$. In the present simulation, $\boldsymbol{H}_{\rm dip}^{\rm total}$ is quantitatively given by a summation of equation (1), instead of equations (6) and (9) for discrete particles. To simulate EMR experiments, $\boldsymbol{H}_{\rm ext}$ is defined by the following equation:

$$\boldsymbol{H}_{\rm ext} = \boldsymbol{H}_{\rm ext}^{\rm sw} + \boldsymbol{H}_{\rm p}\sin(2\pi\nu t), \tag{11}$$

where $\boldsymbol{H}_{\rm ext}^{\rm sw}$ is a dc sweeping and $\boldsymbol{H}_{\rm p}\sin(2\pi\nu t)$ is an ac irradiation field for EMR. $\boldsymbol{H}_{\rm ext}^{\rm sw}$ and $\boldsymbol{H}_{\rm p}$ satisfy $\boldsymbol{H}_{\rm ext}^{\rm sw}\cdot\boldsymbol{H}_{\rm p} = 0$. In the sine function, t is time and ν is frequency.

For the sake of simplicity, we use a three-dimensional (3D) periodic lattice of magnetization as shown in figure 1(b). The Ni particles are arranged in a $9 \times 9 \times 5$ lattice with the lattice spacing r_0. The lattice spacing r_0 in the present model is assigned to the interparticle distance. We directly solve the LLG equation for the magnetization $\boldsymbol{m}_i$ of the ith particles 8 nm in diameter, which is very similar to d_{ave} of Ni particles studied in the experiments. The magnetization $\boldsymbol{m}_i$ is given by $\boldsymbol{m}_i = \mu_s 2\pi d_i^3/3a^3$ emu, where d_i is the diameter of the particle, a is the lattice constant of bulk fcc-Ni and μ_s is the magnetic moment of an Ni atom. When $d_i = 8$ nm, m_i is 1.3×10^{-16} emu. The α of a nanoparticle in equation (10) is set to be 0.01 in this study [43].

In the x and y directions, the periodic boundary condition is applied to take account of the symmetry of the dipolar field. On the other hand, the open boundary condition is provided in the z direction to consider the effect of the composite film thickness. These boundary conditions allow us to regard the model described in figure 1(b) as a thin film. The numerical calculation of equation (10) is carried out using the forward differential method. The time step Δt in the differential equation is defined as $\Delta t \nu = 9 \times 10^{-4}$. The sweeping field $\boldsymbol{H}_{\mathrm{ext}}^{\mathrm{sw}}$ was applied for the directions $\theta = 0°$ or 90°. The frequency and the amplitude of an irradiation field are defined as $\nu/(\gamma H_0) = 1.6$ and $H_{\mathrm{p}}/H_0 = 1.6 \times 10^{-4}$, respectively. The initial direction of magnetization is uniform in the z direction for $\theta = 0°$ and in the x direction for $\theta = 90°$.

The magnetic moment $\boldsymbol{m}$ of the composite film is obtained from a summation $\boldsymbol{m} = \sum \boldsymbol{m}_i$. The $\boldsymbol{m}$ precesses around the $\boldsymbol{H}_{\mathrm{ext}}^{\mathrm{sw}}$ axis and the microwave power is absorbed by the irradiation of H_{p}. Thus, the value $\boldsymbol{m} \cdot \boldsymbol{H}_{\mathrm{p}}$ gives the absorption of the composite film. By using $\boldsymbol{m} \cdot \boldsymbol{H}_{\mathrm{p}}$, the motion of the moment is expressed as

$$m_{H_{\mathrm{p}}} = \frac{\boldsymbol{m} \cdot \boldsymbol{H}_{\mathrm{p}}}{m_{\mathrm{s}} H_{\mathrm{p}}}, \tag{12}$$

which is a projection of a magnetization vector in the H_{p} direction. m_{s} is the saturation magnetization of the Ni particle.

The calculated $m_{H_{\mathrm{p}}}$ as a function of time is plotted in figures 2(a) and (b) when $r_0 = \infty$ and $\theta = 0°$, where $r_0 = \infty$ corresponds to a magnetically isolated particle. Figure 2(a) exhibits the time evolution of $m_{H_{\mathrm{p}}}$ for the on-resonance state ($H_{\mathrm{ext}}^{\mathrm{sw}} = H_0$). The amplitude of the oscillation increases gradually until 6 ns where it reaches its equilibrium. However, for the off-resonance state ($H_{\mathrm{ext}}^{\mathrm{sw}} = 1.09 H_0$), the amplitude of the oscillation is suppressed as shown in figure 2(b). Figure 2 demonstrates that we have succeeded in observing the precession at the resonance in numerical simulations. The calculated value of absorption $m_{H_{\mathrm{p}}}$ is plotted as a function of $H_{\mathrm{ext}}^{\mathrm{sw}}$, forming the absorption lineshape. This line profile is analyzed by fitting it to a Lorentzian lineshape.

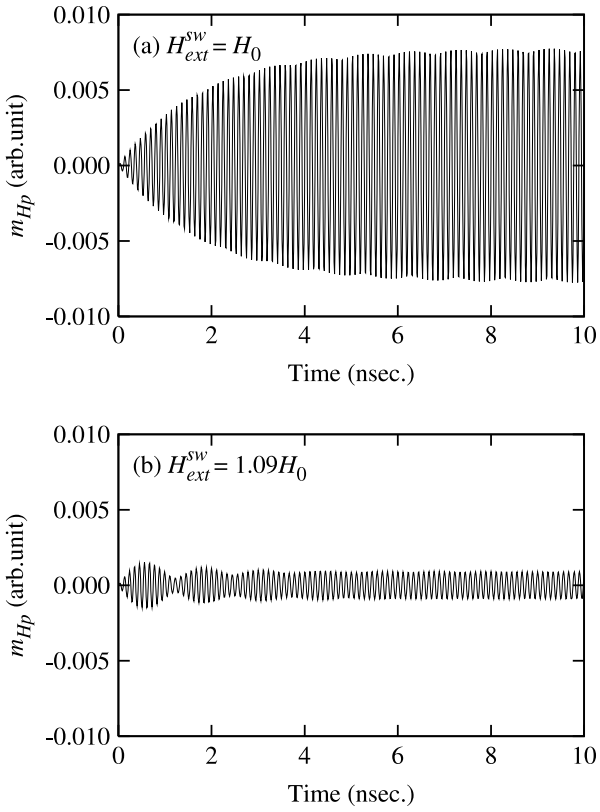

Figure 2. Dynamic motion of magnetization in a composite film for (a) resonance state and (b) off-resonance state. A swept external magnetic field ($H_{\mathrm{ext}}^{\mathrm{sw}}$) is indicated. The particles are magnetically isolated ($r_0 = \infty$). This result corresponds to the perpendicular configuration.

4. Experimental procedures

Detailed procedures for embedding metallic Ni nanoparticles in pyromellitic dianhydride-oxydianiline (PMDA-ODA)-type polyimide (PI) films (Kapton 200-H) were described in our previous articles [31, 32]. Briefly, PI films were treated with aqueous potassium hydroxide (KOH) (5 mol dm^{-3}) for 7 min and were subsequently immersed in aqueous $NiCl_2$ (50 mmol dm^{-3}) in order to adsorb Ni^{2+} by ion-exchange reaction. The concentration of adsorbed Ni^{2+} (N) estimated by inductively coupled plasma (ICP) atomic emission spectroscopy was 1972.5×10^{-9} mol cm^{-2}. The adsorption of Ni^{2+} was followed by thermal annealing in an H_2 gas. The films were annealed at 300 °C for 0–130 min. The Ni^{2+} in the films were completely reduced to Ni atoms at 300 °C, leading to the growth of the metallic Ni nanoparticles [34]. The hydrogen-induced reduction thus yielded surface nanocomposite layers consisting of Ni nanoparticles embedded in PI matrices.

In order to evaluate the thickness of the composite layers and diameter of the Ni nanoparticles, the cross sections of the films were observed using a transmission electron microscope (TEM) operated at 200 kV. Specimens for the cross-sectional TEM studies (100 nm in thickness) were prepared by the standard procedure that includes an embedding of the films in epoxy resin and a sectioning with an ultra-microtome.

EMR studies were carried out at room temperature using a conventional X-band ($\nu = 9.45$ GHz) electron spin resonance spectrometer equipped with a cylindrical TE_{011} cavity. The films were cut into circular discs (3 mm in diameter). They were held in either parallel or perpendicular orientation to the sample plane of the dc sweeping magnetic field ($H_{\mathrm{ext}}^{\mathrm{sw}}$) in the

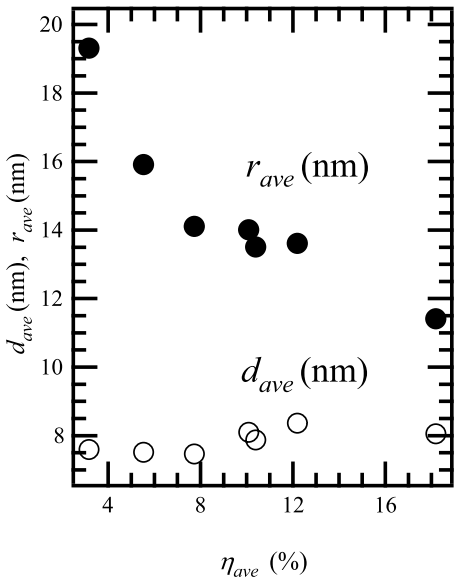

Figure 3. The observed average diameter d_{ave} (open circles) and calculated average interparticle spacing r_{ave} (solid circles) are plotted as a function of the average volume fraction of Ni (η_{ave}).

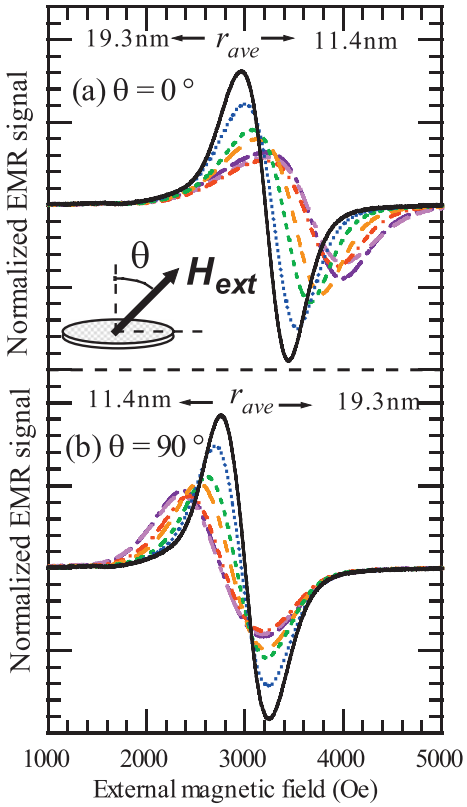

Figure 4. EMR signals with various r_{ave} in (a) the perpendicular ($\theta = 0°$) and (b) parallel ($\theta = 90°$) configurations. A black solid line corresponds to $r_{ave} = 19.3$ nm. The line color changes to red as r_{ave} decreases.

(This figure is in colour only in the electronic version)

cavity; the perpendicular and parallel orientation corresponds to the $\theta = 0°$ and $\theta = 90°$ configuration in this paper. H_{ext}^{sw} was swept from 0 to 10 kOe. A standard field modulation technique is used so that the obtained signal corresponds to the first field derivative of the absorbed microwave power.

5. Results and discussion

5.1. Experimental results

Cross-sectional TEM observation showed that spherical fcc-Ni nanoparticles about 8 nm in diameter were grown in the surface composite layers of PI films [32]. The average particle diameter (d_{ave} (nm)) is fixed around 8 nm for all samples [34]. However, the average thickness of the composite layer (t_{ave} (μm)) observed by TEM decreases from 4.09 to 0.714 μm as the annealing time increases from 0 to 130 min. The shrinkage of the composite layers originates from the thermal decomposition of PI matrices by Ni nanoparticles as a catalyst, vaporization of generated oligomeric (low molecular weight) molecules and the volume loss of the matrices during annealing [31]. Using observed t_{ave} and the amount of adsorbed Ni^{2+} ($N = 1972.5 \times 10^{-9}$ mol cm^{-2}) determined by the ICP before annealing, we can calculate the average volume fraction (η_{ave}) of Ni particles in the composite layer. The η_{ave} (%) is calculated by $\eta_{ave} = (N \times 58.7 \times 100)/(t_{ave} \times 8.91 \times 10^{-4})$ using the atomic weight of Ni (58.7) and the density of bulk fcc-Ni (8.91 (g cm^{-3})). Since t_{ave} decreases in spite of the same N in all samples, η_{ave} increased from 3.2 to 18.2% with increasing annealing time.

η_{ave} is a function of d_{ave} and an average center-to-center interparticle spacing r_{ave} ($\eta_{ave} \propto (d_{ave}/r_{ave})^3$). Therefore, an increase in η_{ave} at a fixed d_{ave} corresponds to a decrease in r_{ave}. If we assume a simple 3D arrangement of the Ni nanoparticles with d_{ave} occupying the sites of a periodic cubic lattice in the film, as shown in figure 1(b), the values of r_{ave} in the present samples can be roughly estimated from the value of η_{ave}. In figure 3, the evaluated r_{ave} are plotted as a function of η_{ave} (solid circles). The d_{ave} is also plotted in the same figure (open circles). In the present samples ($d_{ave} \sim 8$ nm), an increase in η_{ave} from 3.2 to 18.2% corresponds to a decrease in r_{ave} from 19.3 to 11.4 nm. Figure 3 clearly shows that we have succeeded in decreasing r_{ave} between the Ni particles, which maintain a fixed d_{ave}.

Figure 4 exhibits experimental EMR signals with $\nu = 9.45$ GHz for various r_{ave}. The inset in figure 4(a) schematically illustrates the sample configuration in the external field. Figure 4(a) shows EMR signals for the perpendicular ($\theta = 0°$) configuration. Figure 4(b) shows the signals for the parallel ($\theta = 90°$) configuration. In both configurations, the signal for $r_{ave} = 19.3$ nm is observed around 3000 Oe. Figure 4(a) shows that the resonance field H_0' of the signal for the $\theta = 0°$ configuration shifts to the higher field side as r_{ave} decreases down to 11.4 nm. In contrast, the signal for the $\theta = 90°$ configuration shifts to a lower field with decreasing r_{ave} (figure 4(b)). We see that the signal becomes broad with decreasing r_{ave} in both configurations.

Figure 5(a) shows H_0' plotted as a function of r_{ave}. Solid squares correspond to the H_0' data for the $\theta = 0°$ configuration and open squares to the data for the 90° configuration. H_0 is indicated by a dashed line at 3040 Oe for 9.45 GHz. In

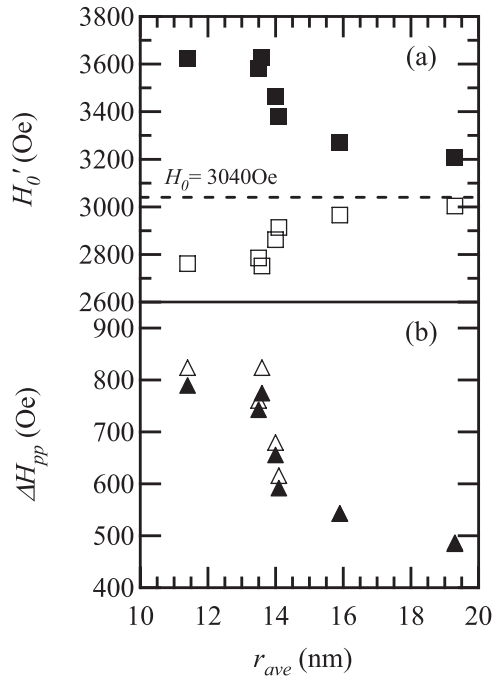

Figure 5. The interparticle spacing r_{ave} versus (a) an apparent resonance field H_0' and (b) a peak-to-peak resonance signal width ΔH_{pp}. The solid symbols correspond to the perpendicular ($\theta = 0°$) configurations. The open symbols correspond to the parallel ($\theta = 90°$) configurations. The resonance field for an isolated spherical Ni particle is also indicated as H_0.

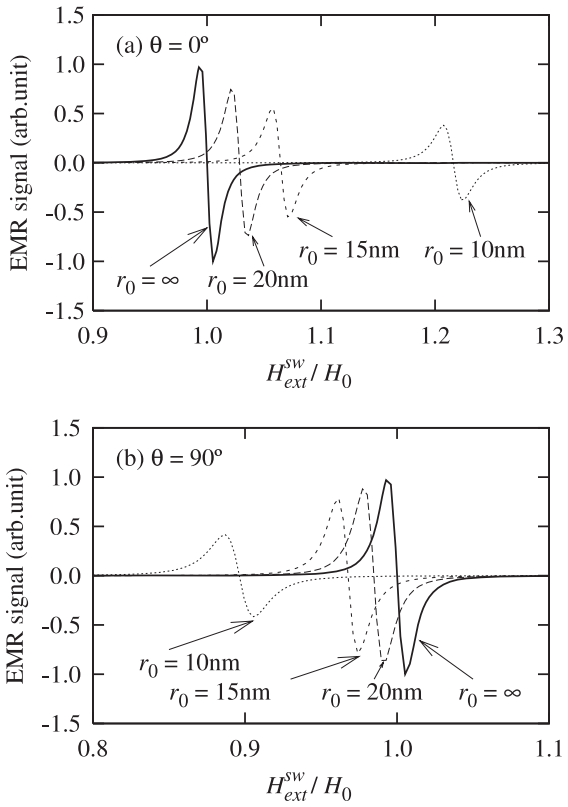

Figure 6. Calculated EMR signals in (a) the perpendicular ($\theta = 0°$) and (b) parallel ($\theta = 90°$) configurations as a function of H_{ext}^{sw}/H_0.

figure 5(b), the peak-to-peak linewidth (ΔH_{pp}) of the signal is plotted. Solid triangles correspond to the data for $\theta = 0°$ configurations. Open triangles correspond to those for $\theta = 90°$ configurations. As r_{ave} decreases ΔH_{pp} increases from about 500 to 800 Oe.

In the following section, based on a numerical simulation of the EMR in interacting Ni nanoparticles, we address these features of decreasing interparticle spacing observed in experiments: (i) a significant shift of the resonance field and (ii) an increase in the linewidth of the EMR signals in both configurations.

5.2. Resonance field

We carried out numerical simulations for 8 nm Ni nanoparticle systems, in which the interparticle distance r_0 is set to 10, 15 and 20 nm, and ∞. A decrease in r_0 leads to an increase in the dipole interaction between nanoparticles in a composite film. The derivative curves of the calculated absorption lines correspond to calculated EMR signals. The calculated EMR signals for the $\theta = 0°$ configuration are shown in figure 6(a) and that for the $\theta = 90°$ configurations in figure 6(b). In figure 7, the shift variation of the resonance field $\delta H_0 = H_0' - H_0$ in the simulation is plotted as a function of the inverse of interparticle distance $1/r_{ave}$. The solid line corresponds to the calculated δH_0 for the $\theta = 0°$ configuration and the dashed one to that for the $\theta = 90°$ configuration. The experimentally observed δH_0 is also plotted in the same figure; solid squares are assigned to the measured δH_0 for the $\theta = 0°$

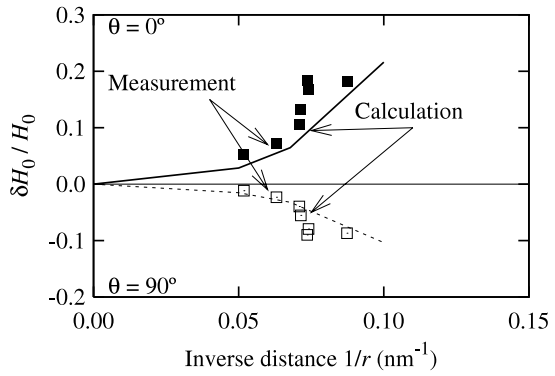

Figure 7. Shift variation of the resonance field (δH_0) plotted as a function of the inverse of the interparticle distance of Ni particles. $\theta = 0°$ corresponds to the perpendicular configuration. $\theta = 90°$ corresponds to the parallel configuration. The solid and open squares show measured δH_0 at $\theta = 0°$ and 90°, respectively. The solid and dashed lines exhibit the calculated data at $\theta = 0°$ and $\theta = 90°$, respectively.

configuration and open squares to the δH_0 for the $\theta = 90°$ configuration. We see in figure 7 that the shift of the resonance field obtained in the simulation quantitatively agrees with the measured one. The present results clearly show that the shift of the resonance field (δH_0) is attributed to an increase in the dipole interactions. The major difference of the measured results from the calculated ones could be caused by random distribution of the nanoparticles in the experiment [41, 42]. It

is worth noting here that $|\delta H_0|/H_0$ for the $\theta = 0°$ configuration is almost twice as large as that for the $\theta = 90°$ configuration. This was predicted by equations (6) and (9) in section 2 [32].

A shift of the resonance field depending on the direction of applied magnetic field is well known in ferromagnetic resonance of continuous films [37]. The shift is caused by the demagnetization field, which originates from the summation of dipole fields between the magnetic atoms in the films [44]. In the present nanoparticle systems, we may draw a similar picture; dipolar fields between discrete magnetic nanoparticles generate the demagnetization field in the composite film, leading to a shift of the resonance field. However, the shift variation for nanoparticle systems is smaller than that for the continuous ferromagnetic films [32].

In a continuous film, strong exchange interaction connects neighboring spins and the dipole field can be treated as uniform in the film. As described in the classical Heisenberg spin model, the exchange interaction depends only on the angle between neighboring spins. The interacting field is independent of the direction of spins. In other words, the degree of freedom is limited to a very small number. The system thus behaves as if there was a single spin under a strong applied field, enabling us to apply a single spin approximation for representing a continuous film. In contrast, in the discrete nanoparticle systems, the magnetization in a single particle is weakly connected to other particles by the dipole interaction. As in equation (1), the magnetic dipole field shows a strong angular dependence, because the sign of the dipole field is dependent on the product of magnetization vector $\boldsymbol{m}$ and position vector $\boldsymbol{r}$. Therefore, the dipole interactions between particles are not uniform; the nanoparticle system is a dynamic many-bodied system.

Additionally, the static approximation is inadequate in the quantitative discussion. The limit of the static approach affects the resonance linewidth in particular. It is reported that, when the external field is applied in parallel to the continuous film plane, i.e. $\theta = 90°$ configuration, a decrease in the film thickness leads to a decrease in the resonance linewidth [45]. This is explained by a decrease in the demagnetization field. In contrast, in the composite films, a smaller interparticle distance r_{ave} and r_0, which correspond to a thinner composite film in the present study, brings about an increase in linewidth as discussed in the next subsection. Therefore, the decrease in the demagnetization field does not explain an increase in linewidth in the interacting nanoparticle systems. We need to gain a clearer understanding of the dipole field in nanoparticle systems within the framework of the dynamic analysis in order to reveal the origins of the broadening of the EMR signals.

5.3. Signal linewidth

We consider the influence of the magnetic dipole field on the linewidth (ΔH_{pp}) of the EMR signal. Figure 8 shows the normalized linewidth (ΔH_{pp}) obtained in experiments and simulation plotted as a function of $1/r_{\mathrm{ave}}$. In the experimental result, the linewidth ΔH_{pp} increases with increasing $1/r_{\mathrm{ave}}$ in both configurations. This variation of linewidth is also reproduced by the numerical simulation, although the variation

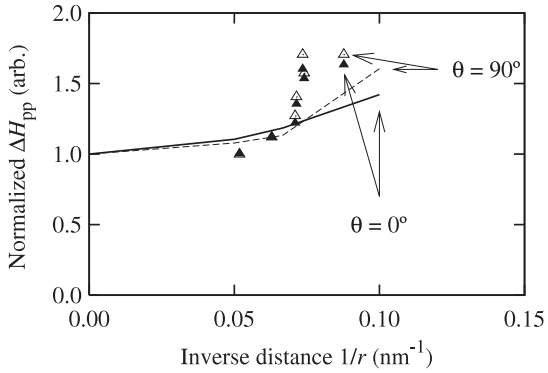

Figure 8. The normalized linewidth (ΔH_{pp}) plotted as a function of the inverse of the interparticle distance of Ni particles. $\theta = 0°$ corresponds to the perpendicular configuration. $\theta = 90°$ corresponds to the parallel configuration. The solid and open triangles show measured ΔH_{pp} at $\theta = 0°$ and $\theta = 90°$, respectively. The solid and dashed lines exhibit the calculated data at $\theta = 0°$ and $\theta = 90°$, respectively.

in the experiment is much larger than that in the simulation at a large $1/r_{\mathrm{ave}}$.

We offer plausible explanations for a larger EMR linewidth with decreasing interparticle spacing observed in the experiment. The small interparticle distance in the composite film gives rise to the strong dipole fields between the particles for any direction of the external applied field. The influence of the dipole broadening is thus significant in the composite system [46]. The measured signals are, however, much broader as shown in figure 8. Another possibility is the inhomogeneity in the nanocomposite. In a continuous film, the inhomogeneity of internal magnetic field broadens the linewidth of ferromagnetic resonance [47]. The inhomogeneity of a shape anisotropy, which is originated from the inhomogeneous dipole field, is particularly an origin of a large linewidth [48]. In a nanocomposite film, we first consider the distribution of particle diameters. The magnetization values m_i of particles are randomly distributed within $(1 \pm \delta_m)\bar{m}$, where $\bar{m}$ is the averaged magnetization of particles and δ_m defines the range of a deviation. $\delta_m = 0.15$ and 0.30 are numerically examined in the present model calculation. For spherical particles, $\delta_m = 0.15$ corresponds to 5% deviation from the averaged diameter and $\delta_m = 0.30$ to 10% deviation from the averaged diameter. The experimentally observed deviation from d_{ave} was about 15%.

The calculated absorption line profiles for $\delta_m = 0, 0.15$ and 0.30 are shown in figure 9. In the calculations, $H_{\mathrm{ext}}^{\mathrm{sw}}$ is applied in the $\theta = 0°$ direction and the interparticle distance $r_0 = 10$ nm. The line profile is normalized by the maximum value. The linewidth ($\Delta H_{\mathrm{pp}}/H_0$) increases with δ_m, even if the damping factor α is fixed at 0.01. The figure clearly shows that a large distribution of particle diameters brings about broadening. The deviation of m_i from the average value causes a large distribution of $H_{\mathrm{dip}}^{\mathrm{total}}$ as expressed in equation (1). The change of the magnetic dipole fields between particles expands the absorption linewidth of the EMR. In this sense, the inhomogeneity for an interparticle distance may also influence the absorption linewidth, because the strength of the

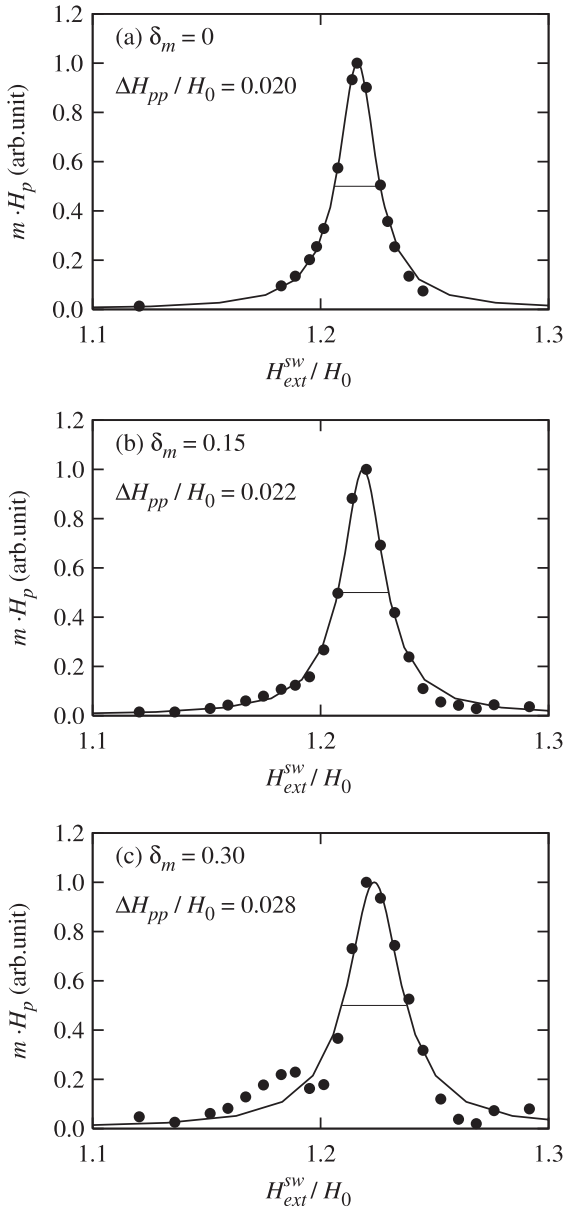

Figure 9. Peak profiles of inhomogeneous magnetization in the composite film with the interparticle distance $r_0 = 10$ nm as a function of $H^{\rm sw}_{\rm ext}/H_0$ in the perpendicular ($\theta = 0°$) configuration. The magnetization of particles ranges within $(1 \pm \delta_m)\bar{m}$. (a) $\delta_m = 0$, (b) $\delta_m = 0.15$ and (c) $\delta_m = 0.30$. The peak width ($\Delta H_{\rm pp}/H_0$) is also indicated.

dipole field is proportional to r^{-3} as shown in equations (2)–(4). Particularly for the region of small $r_{\rm ave}$, the effect of the inhomogeneity in particle position must become more significant. Accordingly, composite films with high volume fraction would show a large linewidth. Owing to the Ewalt sum, the simulation on randomly distributed particles is quite difficult, however.

5.4. Parallel and perpendicular components of dipolar field

Figure 8 shows that the linewidth $\Delta H_{\rm pp}$ becomes broad when $1/r_{\rm ave}$ increases. The increase in $1/r_{\rm ave}$ leads to a peak

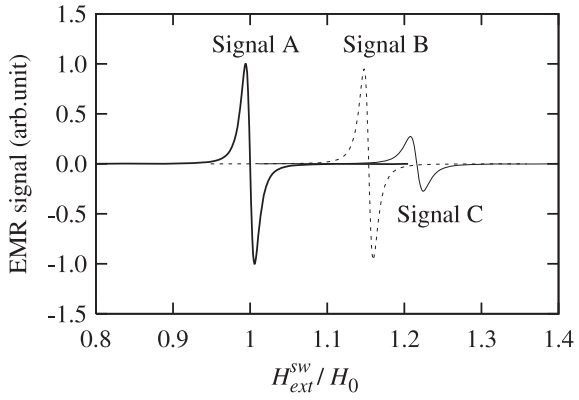

Figure 10. The line profile of EMR signal under influence of the magnetic dipole field in the $\theta = 0°$ configuration. The bold line describes the precession of isolated particle having resonance field H_0 (signal A). The dashed line stands for the case of $H_0' = H_0 + H_\parallel$, in which $H_\perp$ is artificially $H_\perp = 0$ (signal B). The solid thin line represents the case with a finite $H_\perp$ (signal C).

shift δH_0, which is originated from the shape anisotropy of the composite films and is equivalent to the dipole field as shown in figure 7. $\boldsymbol{H}^{\rm total}_{\rm dip}$ for both the $\theta = 0°$ and the $\theta = 90°$ configurations consists of two components. The major component of $\boldsymbol{H}^{\rm total}_{\rm dip}$ is parallel to the applied field $\boldsymbol{H}^{\rm sw}_{\rm ext}$. The finite value of $m_{H_{\rm p}}$ additionally generates a perpendicular component of $\boldsymbol{H}^{\rm total}_{\rm dip}$ against $\boldsymbol{H}^{\rm sw}_{\rm ext}$ in the resonance state. Hereafter, the parallel and perpendicular components of $\boldsymbol{H}^{\rm total}_{\rm dip}$ against $\boldsymbol{H}^{\rm sw}_{\rm ext}$, i.e. the precession axis, are expressed as $H_\parallel$ and $H_\perp$.

In the equilibrium state of precession, $H_\parallel$ remains constant independent of time. The simple calculation of the demagnetizing field uses only $H_\parallel$, because of $H_\parallel \gg H_\perp$. This corresponds to a static approximation used in the Kittel equation. On the other hand, even though the absolute value $|H_\perp|$ is constant, the field vector $\boldsymbol{H}_\perp$ oscillates in direction during the precession. To account for $H_\perp$, a time-dependent calculation is necessary. This is a dynamic approximation for the magnetic dipole field in a resonance model, which represent the present experiments exactly. In the case of nanocomposite material, the dynamic approximation is necessary to understand the resonance condition, because the dipole interaction among particles is not uniform in space and it is not constant in time.

We numerically studied the dynamic effect of $H_\perp$ on the line profile of the EMR signal for the case of $\theta = 0°$ with $r_0 = 10$ nm as shown in figure 10. A bold line corresponds to the precession of the isolated particles having resonance field H_0 (signal A). A dashed line stands for the case of $H_0' = H_0 + H_\parallel$, in which $H_\perp$ is artificially $H_\perp = 0$ (signal B). A solid thin line represents the case for a finite $H_\perp$ (signal C). In figure 10, the peak-to-peak height of signal A is normalized to unity. Signal B shows that $\Delta H^{\rm (B)}_{\rm pp}/\Delta H^{\rm (A)}_{\rm pp} = 1.03$; the linewidth of signal B is almost the same as that of signal A when we ignore the component $H_\perp$ in the dipole field. In contrast to signal B, the width of signal C is broadened by the influence of a dipole field, which consists of both $H_\parallel$ and $H_\perp$; $\Delta H^{\rm (C)}_{\rm pp}/\Delta H^{\rm (A)}_{\rm pp} = 1.42$.

$H_\perp$ also affects the resonance field. The shift of a resonance field for signal B is $\delta H^{(B)}/H_0 = 0.154$, which is equivalent to $H_\parallel/H_0$. This is smaller than the measured value as shown in figure 7. For signal C, on the other hand, $\delta H^{(C)}/H_0 = 0.216$, which gives $\delta H^{(C)} > \delta H^{(B)} = H_\parallel$ and is comparable to the measured value in figure 7. We thus conclude that $H_\perp$ critically influences both the resonance field and linewidth. In particular, the linewidth cannot be reproduced without $H_\perp$. In contrast to $H_\perp$, the influence of $H_\parallel$ is limited to the shift of the resonance field.

It is worth noting that δH is not given by the simple summation of $H_\parallel + H_\perp$, although the magnitude of $H_\perp$ is very small ($H_\perp/H_0 = 5 \times 10^{-4}$). Since a decrease in r_0 leads to an increase in $H_\perp$, a smaller r_0 brings about a weak EMR signal. We conclude that the dynamic effect of the perpendicular component $H_\perp$ of the dipolar field is among the origins of the broader EMR signal despite the very small amplitude of $H_\perp$ compared to that of $H_\parallel$. The dynamic effect of a dipole field significantly changes the resonance conditions through the nonlinearity of magnetic nanoparticle systems.

6. Conclusions

Metallic Ni nanoparticles were embedded in polymer matrices forming nanocomposite films. The average particle diameter d_{ave} and the average interparticle distance r_{ave} were independently controlled. We measured the EMR signals of nanocomposite films with $d_{ave} = 8$ nm and various r_{ave}. In addition, we constructed the micromagnetic model to directly solve the LLG equation of the magnetization of the nanoparticle systems with mutual dipolar interaction.

The present study shows that, for discrete and regularly arrayed nanoparticle systems, the exact treatment of the dipole field and dynamic analysis are indispensable for quantitative discussion on the resonance field position and linewidth of EMR signals. Micromagnetic calculations using the exact treatment of the dipole field successfully reproduced the shift of the resonance field and the broadening of the resonance signal with decreasing interparticle spacing r_{ave} observed in experiments. The shift and broadening thus mainly arises from an increase of magnetic dipole fields due to a decrease of r_{ave}, although an inhomogeneous dipolar field induced by particle diameter and spatial distribution may cause further broadening. The latter origin of line broadening is, however, difficult to treat exactly in the calculations.

Most significantly, the dipole field $\boldsymbol{H}_{dip}^{total}$ in the nanoparticle systems consists of parallel $H_\parallel$ and perpendicular components $H_\perp$ against the precession axis. The influence of $H_\parallel$ is limited to the peak shift. In contrast, we reveal that $H_\perp$ critically influences both the resonance field and linewidth, despite the comparatively small magnitude of $H_\perp$.

Acknowledgments

The authors thank T Kashiwagi, H Shinkai and S Ikeda for their valuable contributions in the initial stage of this work. The authors also acknowledge H Nawafune, H Yanagi, H Takayama, K Takeuchi and S Ushioda for their fruitful discussions. ST acknowledges support from PRESTO, JST.

References

[1] Smith D R, Pendry J B and Wiltshire M C K 2004 *Science* **305** 788
[2] Veselago V G 1968 *Sov. Phys.—Usp.* **10** 509
[3] Pendry J B 2000 *Phys. Rev. Lett.* **85** 3966
[4] Parazzoli C G, Greegor R B, Neilsen J A, Thompson M A, Li K, Vetter A M and Vier D C 2004 *Appl. Phys. Lett.* **84** 3232
[5] Schurig D, Mock J J, Justice B J, Cummer S A, Pendry J B, Starr A F and Smith D R 2006 *Science* **314** 977
[6] Pendry J B, Holden A J, Robbins D R and Stewart M J 1999 *IEEE Trans. Microw. Theory Tech.* **47** 2075
[7] Smith D R, Padilla W J, Vier D C, Nemat-Nasser S C and Schultz S 2000 *Phys. Rev. Lett.* **84** 4184
[8] Chui S T and Hu L 2002 *Phys. Rev.* B **65** 144407
[9] Chikazumi S 1997 *Physics of Ferromagnetism* (Oxford: Oxford University Press)
[10] Konchits A A, Motsnyi F V, Petrov Yu N, Kolesnik S P, Yefanov V S, Terranova M L, Tamburri E, Orlanducci S, Sessa V and Rossi M 2006 *J. Appl. Phys.* **100** 124315
[11] Schmool D S, Rocha R, Sousa J B, Santos A M, Kakazei G N, Garitaonandia J S and Lezama L 2007 *J. Appl. Phys.* **101** 103907
[12] Fittipaldi M, Sorace L, Barra A-L, Sangregorio C, Sessoli R and Gatteschi D 2009 *Phys. Chem. Chem. Phys.* **11** 6555
[13] Noginova N, Chen F, Weaver T, Giannelis E P, Bourlions A B and Atsarkin V A 2007 *J. Phys.: Condens. Matter* **19** 246208
[14] Noginova N, Weaver T, Giannelis E P, Bourlions A B, Atsarkin V A and Demidov V V 2008 *Phys. Rev.* B **77** 014403
[15] Noginov M M, Noginova N, Amponsah O, Bah R, Rakhimov R and Atsarkin V A 2008 *J. Magn. Magn. Mater.* **320** 2228
[16] Rao S S, Padmanabhan B, Elizabeth S, Bhat H L and Bhat S V 2008 *J. Phys. D: Appl. Phys.* **41** 155011
[17] Rao S S, Padmanabhan B, Elizabeth S, Bhat H L and Bhat S V 2009 *J. Phys. D: Appl. Phys.* **42** 075004
[18] Sahoo S, Petracic O, Kleemann W, Stappert S, Dumpich G, Nordblad P, Cardoso S and Freitas P P 2003 *Appl. Phys. Lett.* **82** 4116
[19] Buchanan K S, Krichevsky A, Freeman M R and Meldrum A 2004 *Phys. Rev.* B **70** 174436
[20] Cowburn R P and Welland M E 2000 *Science* **287** 1466
[21] Skumryev V, Stoyanov S, Zhang Y, Hadjipanayis G, Givord D and Nogués J 2003 *Nature* **423** 850
[22] Butera A, Zhou J N and Barnard J A 1999 *Phys. Rev.* B **60** 12270
[23] Ebels U, Duvail J-L, Wigen P E, Piraux L, Buda L D and Ounadjela K 2001 *Phys. Rev.* B **64** 144421
[24] Jung S, Ketterson J B and Chandrasekhar V 2002 *Phys. Rev.* B **66** 132405
[25] Tomita S, Hagiwara M, Kashiwagi T, Tsuruta C, Matsui Y, Fujii M and Hayashi S 2004 *J. Appl. Phys.* **95** 8194
[26] Arias R and Mills D L 2004 *Phys. Rev.* B **70** 104425
[27] Arias R, Chu P and Mills D L 2005 *Phys. Rev.* B **71** 224410
[28] Laroze D and Vargas P 2006 *Physica* B **372** 332
[29] Jensen P J and Pastor G M 2003 *Phys. Rev.* B **68** 184420
[30] Puntes V F, Gorostiza P, Aruguete D M, Bastus N G and Alivisatos A P 2004 *Nat. Mater.* **3** 263
[31] Akamatsu K, Shinkai H, Ikeda S, Nawafune H and Tomita S 2005 *J. Am. Chem. Soc.* **127** 7980
[32] Tomita S, Akamatsu K, Shinkai H, Ikeda S, Nawafune H, Mitsumata C, Kashiwagi T and Hagiwara M 2005 *Phys. Rev.* B **71** 180414(R)
[33] Tomita S, Jönsson P E, Akamatsu K, Nawafune H and Takayama H 2007 *Phys. Rev.* B **76** 174432

[34] Tomita S, Akamatsu K, Shinkai H, Ikeda S, Nawafune H, Mitsumata C, Kashiwagi T and Hagiwara M 2005 *MRS Proc.* **853E** I5.10.1
[35] Draaisma H J G and de Jonge W J M 1988 *J. Appl. Phys.* **64** 3610
[36] Cochran J F and Kambersky V 2006 *J. Magn. Magn. Mater.* **302** 348
[37] Kittel C 1995 *Introduction to Solid State Physics* 7th edn (New York: Wiley)
[38] Safonov V L and Bertram H N 2001 *Phys. Rev.* B **63** 094419
[39] Hachemi H, Hachemi A and Louail L 2004 *Mater. Lett.* **58** 824
[40] Mitsumata C and Tomita S 2007 *Appl. Phys. Lett.* **91** 223104
[41] Parker G J, Cerjan C and Hewett D W 2000 *J. Magn. Magn. Mater.* **214** 130
[42] Politi P and Pini M G 2002 *Phys. Rev.* B **66** 214414
[43] Counil G, Kim J-V, Devolder T, Chappert C, Shigeto K and Otani Y 2004 *J. Appl. Phys.* **95** 5646
[44] Nakatani Y, Uesaka Y and Hayashi N 1989 *Japan. J. Appl. Phys.* **28** 2485
[45] Patton C E, Wilts C H and Humphrey F B 1967 *J. Appl. Phys.* **38** 1358
[46] Van Vleck J H 1948 *Phys. Rev.* **74** 1168
[47] Chappert C, Le Dang K, Beauvillain P, Hurdequint H and Renard D 1986 *Phys. Rev.* B **34** 3192
[48] Mizukami S, Ando Y and Miyazaki T 2000 *J. Magn. Soc. Japan* **24** 535